

Galaxy Zoo: A sample of blue early-type galaxies at low redshift^{*}

Kevin Schawinski^{1,2,3,†}, Chris Lintott³, Daniel Thomas⁴, Marc Sarzi⁵, Dan Andreescu⁶, Steven P. Bamford^{4,7}, Sugata Kaviraj³, Sadegh Khochfar^{3,8}, Kate Land³, Phil Murray⁹, Robert C. Nichol⁴, M. Jordan Raddick¹⁰, Anže Slosar¹¹, Alex Szalay¹⁰, Jan VandenBerg¹⁰ and Suhyoung K. Yi¹²

¹Department of Physics, Yale University, New Haven, CT 06511, U.S.A.

²Yale Center for Astronomy and Astrophysics, Yale University, P.O. Box 208121, New Haven, CT 06520, U.S.A.

³Department of Physics, University of Oxford, Oxford OX1 3RH, UK.

⁴Institute of Cosmology & Gravitation, University of Portsmouth, Portsmouth, PO1 2EG.

⁵Centre for Astrophysics Research, University of Hertfordshire, College Lane, Hatfield, Herts AL10 9AB.

⁶LinkLab, 4506 Graystone Ave., Bronx, NY 10471, USA.

⁷Centre for Astronomy and Particle Theory, University of Nottingham, University Park, Nottingham, NG7 2RD, UK.

⁸Max Planck Institut für extraterrestrische Physik, P.O. box 1312, D-85478 Garching, Germany

⁹Fingerprint Digital Media, 9 Victoria Close, Newtownards, Co. Down, Northern Ireland, BT23 7GY, UK.

¹⁰Department of Physics and Astronomy, The Johns Hopkins University, Baltimore, MD 21218.

¹¹Berkeley Center for Cosmological Physics, Lawrence Berkeley National Lab, 1 Cyclotron Road, MS 50-5005, Berkeley, CA 94720.

¹²Department of Astronomy, Yonsei University, Seoul 120-749, Korea.

ABSTRACT

We report the discovery of a population of nearby, blue early-type galaxies with high star formation rates ($0.5 < \text{SFR} < 50 M_{\odot} \text{yr}^{-1}$). They are identified by their visual morphology as provided by Galaxy Zoo for SDSS DR6 and their $u - r$ colour. We select a volume-limited sample in the redshift range $0.02 < z < 0.05$, corresponding to luminosities of approximately L^* and above, and with $u - r$ colours significantly bluer than the red sequence. We confirm the early-type morphology of the objects in this sample and investigate their environmental dependence and star formation properties. Blue early-type galaxies tend to live in lower-density environments than ‘normal’ red sequence early-types and make up $5.7 \pm 0.4\%$ of the low-redshift early-type galaxy population. We find that such blue early-type galaxies are virtually absent at high velocity dispersions above 200 km s^{-1} . Our analysis uses emission line diagnostic diagrams and we find that $\sim 25\%$ of them are actively starforming, while another $\sim 25\%$ host both star formation and an AGN. Another $\sim 12\%$ are AGN. The remaining 38% show no strong emission lines. When present and uncontaminated by an AGN contribution, the star formation is generally intense. We consider star formation rates derived from $H\alpha$, u -band and infrared luminosities, and radial colour profiles, and conclude that the star formation is spatially extended. Of those objects that are not currently undergoing star formation must have ceased doing so recently in order to account for their blue optical colours. The gas phase metallicity of the actively starforming blue early-types galaxies is supersolar in all cases. We discuss the place of these objects in the context of galaxy formation. A catalogue of all 204 blue early-type galaxies in our sample, including star formation rates and emission line classification, is provided.

Key words: galaxies: elliptical and lenticular, galaxies: evolution, galaxies: formation, galaxies: fundamental parameters, galaxies: starburst

^{*} This publication has been made possible by the participation of more than 160,000 volunteers in the Galaxy Zoo project. Their contributions are individually acknowledged at <http://www.galaxyzoo.org/Volunteers.aspx>.

[†] E-mail: kevin@astro.ox.ac.uk

1 INTRODUCTION

Early-type galaxies are a fascinating probe of galaxy formation. Their apparent simplicity is deceiving, since much of the physics that is involved in their formation and evolution is still poorly understood. It is now common practice to divide the galaxy population on a colour-magnitude diagram (e.g. Baldry et al. 2004; Figure 1), where early-type galaxies typically appear to lie on a red sequence while spirals display bluer colours and seem to reside in a ‘blue cloud’ (Chester & Roberts 1964; Bower et al. 1992; Driver et al. 2006; Faber et al. 2007). Morphological early-type galaxies residing in this blue cloud of starforming galaxies are of great importance for our understanding of the formation of early-type galaxies and the build-up of the red sequence. These blue early-type galaxies do provide us with a laboratory to understand the physical processes that underly their evolution (Schawinski et al. 2007b; Salim et al. 2007; Constantin et al. 2008; Schawinski et al. 2009a). Schawinski et al. (2007b), hereafter S07, have already shown that there is a significant population of such blue early-type galaxies at low velocity dispersion.

Samples of blue early-type galaxies have tended to be small, as the most reliable way to identify them is through visual inspection of images. In a seminal study, Huchra (1977a,b) studied the non-Seyfert population of the Markarian catalogue and concludes that these Markarian systems are systematically blue for their morphology, possibly indicating an episode of recent star formation. This sample includes a number of systems classified visually as early-type (E or S0).

Many studies attempt to select large samples by using automated structural parameter measurements, such as concentration to isolate early- and late-type galaxies. However, samples selected by structural quantities do not correspond well to those based on visual morphological classification (van der Wel 2008). Fukugita et al. (2004) found three blue early-type galaxies (two starforming and one hosting an active-galactic nucleus, AGN) with star formation rates (SFR) of 2.9 and 4.8 $M_{\odot}\text{yr}^{-1}$, an order of magnitude fainter than the highest SFR we find. A larger sample of visually classified galaxies is presented in Fukugita et al. (2007), though the question of blue early-type galaxies is not addressed. Early samples of blue galaxies of early-type morphology tended to focus on very low mass systems, such as dEs, which may not be the same as the more massive systems that we can access in the SDSS universe (Kunth et al. 1988; Telles et al. 1997; Doublier et al. 1997). A catalogue of early-type galaxies with emission lines was published by Bettoni & Buson (1987).

In this Paper we present a new sample of 204 blue early-type galaxies populating the extreme blue end of a sample of 3588 nearby early-type galaxies. We thus confirm that blue early-type galaxies with significant amounts of star formation exist but make up only a small fraction of early-types in the low-redshift Universe and investigate their properties in detail. The parent sample is selected by morphology determined by careful and repeated visual inspection. The extreme blue sample is then selected based on $u - r$ optical colour. Our blue early-type galaxies can display intense star-formation, with star-formation rates ranging from $0.5 < \text{SFR} < 50 M_{\odot}\text{yr}^{-1}$, comparable at the low end to typical spiral galaxies and representing at the high end the most intensely starforming early-type galaxies ever detected.

2 SAMPLE PROPERTIES

Our sample of morphological early-type galaxies is drawn from the Galaxy Zoo `clean` catalog (Lintott et al. 2008), which provides us with visual classifications for galaxies from the Sloan Digital Sky Survey Data Release 6 (SDSS DR6; York et al. 2000; Adelman-McCarthy et al. 2008). The Galaxy Zoo classifications of morphology are based on the visual inspection of SDSS images by a large number of independent observers. As described in (Lintott et al. 2008), Galaxy Zoo enlists the help of members of the public to classify the spectroscopic galaxy sample from the Sloan Digital Sky Survey. This selection made only via morphology is crucial when selecting non-passive early-type galaxies. We select all galaxies with spectra in the redshift interval $0.02 < z < 0.05$ and create a volume-limited sample by limiting to an absolute magnitude of $M_r < -20.7$, which is slightly below M_* for low-redshift early-type galaxies ($M_{r,*} = -21.15$, Bernardi et al. 2003). In this volume-limited sample, we then focus on the morphological early-type galaxies. The visual classifications from Galaxy Zoo of the objects presented here (see Section 2.3) should provide robust confirmation of their early-type morphology as the redshift and apparent magnitude limits used are lower than those of Fukugita et al. (2004) and S07. The colours are derived from SDSS `modelMags`, which are optimised for galaxy colours, while the absolute magnitudes are based on the SDSS `petroMag`, which is a good measure of the total light.

2.1 Selection of Blue Early-type Galaxies

On the left-hand side of Figure 1, we plot the optical colour-magnitude relation for the early-type galaxies in our sample. In $u - r$ colour, the majority of early-type galaxies lie on a tight red sequence, while a minority scatters to significantly bluer $u - r$ colours. We fit a Gaussian to the $u - r$ colour of the early-type population in magnitude bins of $dM = 0.33$ mag. Using this fit, we determine the 3σ offset to the red sequence and define as **blue early-type galaxies** those that are below this offset. This strong selection ensures that we are probing the blue extreme of the early-type galaxy population. On Figure 1, we indicate the mean of the red sequence as the solid line and the 3σ offsets as dashed lines. This produces a sample of 204 blue early-type galaxies.

The overall fraction of early-type galaxies that are selected in this volume-limited sample is $5.7 \pm 0.4\%$. This fraction is significantly higher than the 0.23% expected from a 3σ limit of a purely Gaussian distribution; this is due to the fact that the $u - r$ colour-magnitude relation is not a perfect Gaussian, but displays an excessive scatter to bluer colours. The assumption of the colour distribution of the red sequence as a Gaussian is nevertheless a good one and the blue early-types are a sub-population that scatters off this Gaussian. The $5.7 \pm 0.4\%$ fraction is lower than that found by S07, as our selection via extremely blue colours is more stringent than their selection via emission lines. Here we only select those galaxies whose colours are extremely blue, while S07 included early-type galaxies with emission lines that were closer to, or even on, the red sequence. Selecting early-type galaxies with emission lines has a considerable overlap with the colour selection, but there are also numerous early-type galaxies with emission lines that are on the red sequence. These red early-type galaxies mostly show emission lines with LINER-like ratios (see e.g. Graves et al. 2007 and S07). Graves et al. (2007) show that early-types that show LINER emissions tend to be systematically younger than their passive counter-

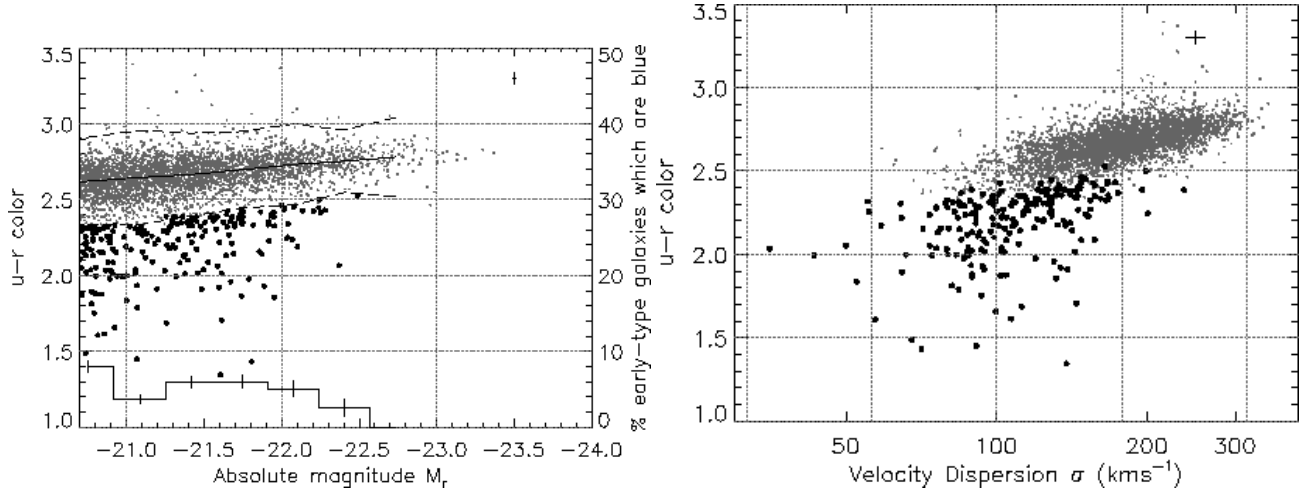


Figure 1. *Left:* We show the optical colour-magnitude relation for our volume-limited sample of morphological early-type galaxies. The solid line represents the mean of a gaussian fit to the red sequence, while the dashed lines indicate the 3σ offset from that mean. We plot all those early-type galaxies above this 3σ offset as small gray points and those below as large black points. On top of this, we plot a histogram of the fraction of early-type galaxies as a function of M_r classified as blue early-type galaxies and the scale is indicated on the right-hand vertical axis. *Right:* We show the colour- σ relation for our sample, indicating galaxies using the same symbols. Blue early-type galaxies have velocity dispersions that are significantly lower than the majority of red early-type galaxies with similar luminosities. As star formation is suppressed, they will move vertically up at a given velocity dispersion as they join the red sequence. Blue early-type galaxies in the low-redshift Universe are thus building the lower-mass end of the red sequence in accordance with downsizing (Thomas et al. 2005). The blue early-type galaxy fraction is a strong function of velocity dispersion and there are *virtually no* blue early-type galaxies above a velocity dispersion of $\sigma = 200 \text{ km s}^{-1}$ (c.f. Schawinski et al. 2006). We indicate the typical 3σ error for the blue early-types in the top right corner.

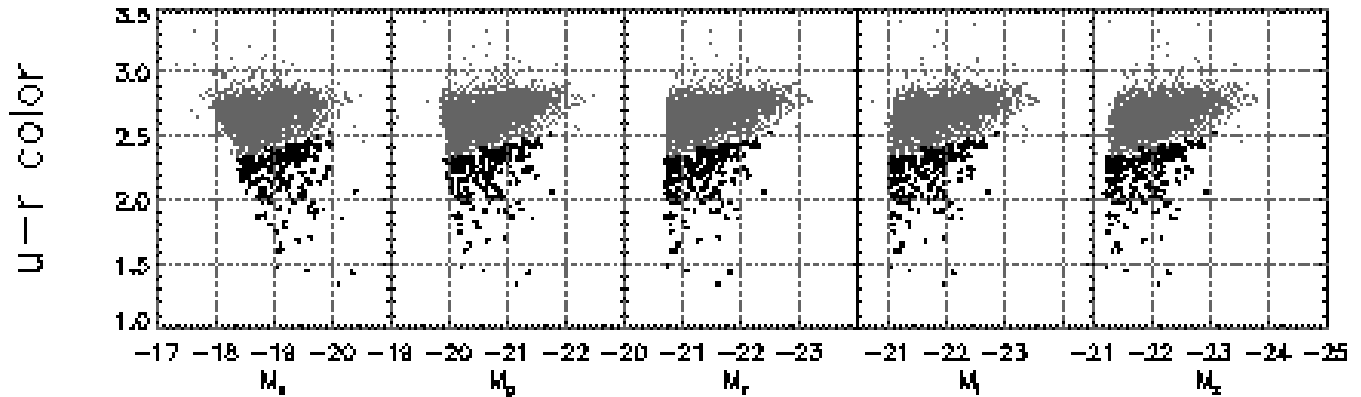


Figure 2. We plot the $u - r$ colour-magnitude relations as a function of all five SDSS filter absolute magnitudes (M_u , M_g , M_r , M_i and M_z) to illustrate the effect on these absolute magnitudes of the young stellar populations present in blue early-type galaxies. In the M_u diagram, the young stellar populations boost the absolute magnitude such that blue early-types are as luminous as the most massive early-type galaxies despite their low velocity dispersion (c.f. Figure 1, left). As we go to redder bands, the absolute magnitude is less and less affected by the young population and the M_z colour-magnitude relation is most similar to the colour- σ diagram. For an in-depth discussion on the selection bias introduced by this, see Section 2.2

parts at the same velocity dispersion. In this Paper, we are probing the extreme end of the active early-type population.

If we plot the colour-magnitude relation as a function of all SDSS bands (see Figure 2), it becomes apparent that the young stellar populations that account for the blue $u - r$ colours affect the absolute magnitude. The u -band is most affected, resulting in absolute magnitudes similar to those of the most massive red sequence early-type galaxies. The z -band is least affected and is more similar to the colour- σ relation. The selection bias introduced by this are discussed in Section 2.2.

2.2 The Faber-Jackson Relation and Sample Bias

The distributions of M_r and σ in Figures 1 and 2 support a picture where blue early-type galaxies are systems containing substantial

young stellar populations with low and intermediate velocity dispersions almost exclusively below $\sigma = 200 \text{ km s}^{-1}$, in accordance with the picture of downsizing (Thomas et al. 2005; Nelan et al. 2005; Bernardi et al. 2005). *There are extremely few blue early-type galaxies with $\sigma > 200 \text{ km s}^{-1}$ in the low-redshift Universe.* The absence of blue early-type galaxies at high velocity dispersions cannot be accounted for by any selection effects.

In Figure 3 we plot the Faber-Jackson relation (Faber & Jackson 1976), we can see that blue early-type galaxies (black points) scatter away from the position of red early-types (gray points). The velocity dispersions of these systems are unaffected by young stellar populations, but their boosting of the absolute magnitude is sufficient to account for the offset. In Figure 3, we use Maraston (2005) models to show the expected fading of stellar populations given a selection of mass fractions and other

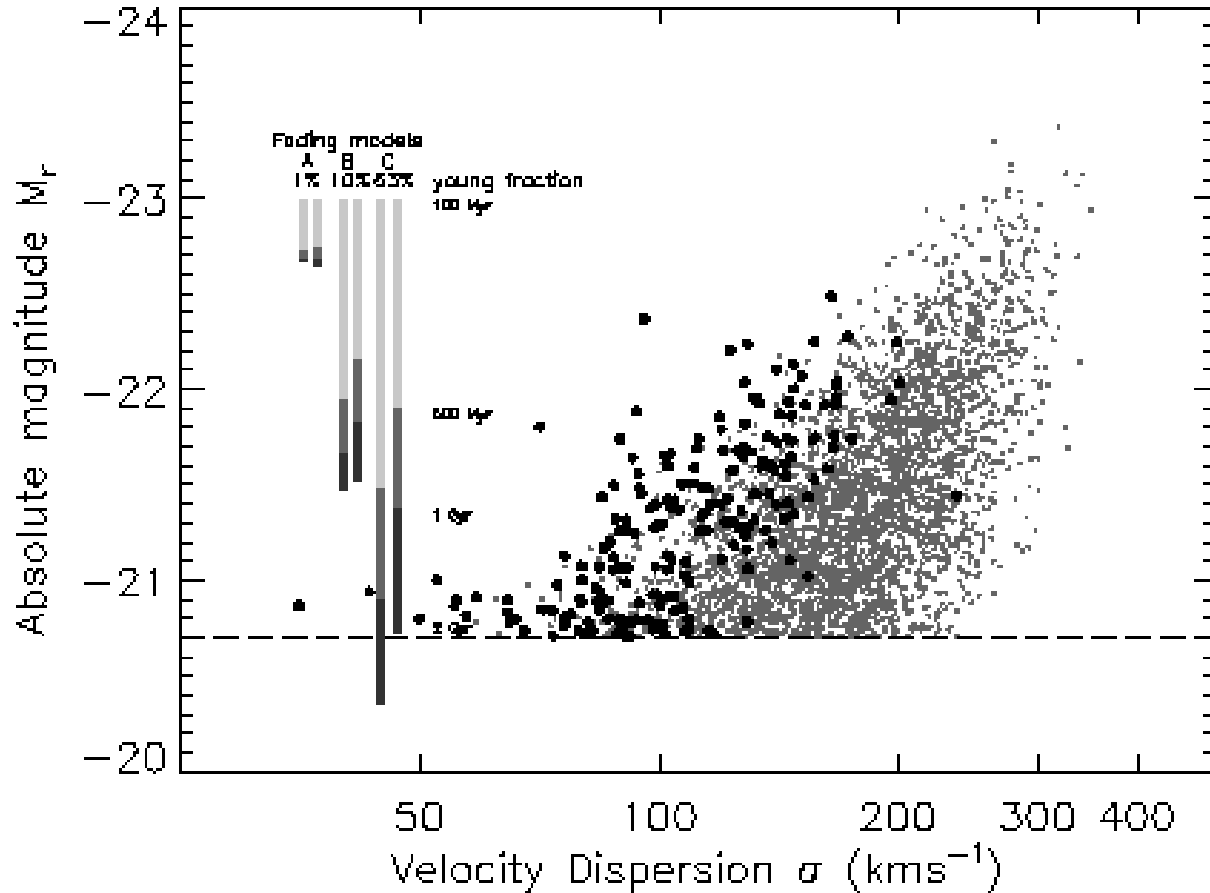


Figure 3. In this Figure, we present the Faber-Jackson relation (Faber & Jackson 1976) for our volume-limited sample of early-type galaxies. The absolute magnitude cut is indicated by the dashed line. As in Figure 1, we indicate red early-type galaxies as small gray points and blue early-type galaxies as larger black points. The blue early-type galaxy population scatters off the locus of their red counterparts. This may lead to selection bias (see Section 2.2) as the more luminous blue early-type galaxies at lower velocity dispersions are put into the volume-limited sample. We indicate how blue early-type galaxies might fade to the Faber-Jackson relation by determining the amount of fading expected from a variety of starburst models. We place a young population of 1%, 10% and 63% mass fraction on top of an 8 Gyr old solar metallicity SSP with $E(B-V) = 0.05$ (Calzetti et al. 2000), corresponding to models A, B and C. We then calculate the expected fading starting from 100 Myr age to 500 Myr, 1 Gyr and 2 Gyr. We use grayscale to indicate these time steps. For each mass fraction, the left bars represent a rapidly declining star formation history where the young burst is modelled as an exponentially declining star formation history with $\tau = 100$ Myr. The right bar represents a $\tau = 1$ Gyr. If these star formation histories roughly represent those of blue early-type galaxies, then a return to the Faber-Jackson relation within ~ 1 Gyr is plausible for starbursts of a few percent by mass.

parameters to show that a declining star formation history will place blue early-type galaxies on the Faber Jackson relation within 1 Gyr.

The boosting of the r -band luminosity will introduce a bias on our selection of a volume-limited sample with $M_r < -20.7$ as blue early-type galaxies at lower velocity dispersion will enter this selection, while red early-type galaxies will not (c.f. Faber Jackson relation, Figure 3). Thus the fraction of blue early-type galaxies of $5.7 \pm 0.4\%$ should be viewed as an upper limit on the blue fraction given our selection. A sample selection that is complete in velocity dispersion encounters the problem that the reliability of the visual inspection decreases as a function of apparent magnitude (Bamford et al. 2008), and so the purity of the sample will be compromised. The blue early-type galaxies presented here are low- to intermediate-mass early-type galaxies, not M^* and more massive systems. In a complete, mass-selected sample, the fraction of blue early-type galaxies at the high-mass end would be low.

2.3 Confirmation of Early-type Morphology

As discussed earlier, this sample of blue early-type galaxies is at lower redshift and apparent magnitude and so the visual classification is highly secure. We present example gri images to illustrate this in Figure 4. We also provide images of a sample of galaxies classified as face-on spirals in the same luminosity and redshift range in Figure 5 for comparison. By using the Galaxy Zoo clean sample, we further ensure that we have only selected galaxies about which a substantial majority of classifiers ($> 80\%$ by weighted vote, see Lintott et al. 2008 for a discussion) concur.

The most relevant comparison for Galaxy Zoo early-types is with those of the MOSES (Morphologically Selected Ellipticals in SDSS; Schawinski et al. 2007b) sample, selected by one professional classifier. Essentially all of the MOSES early-types included in Galaxy Zoo ($> 99.9\%$) were found to be early-type. However, the Galaxy Zoo early-type sample included a small number of galaxies that were not classified as early-type in MOSES; comparison with the sample of Fukugita et al. (2007) who provided detailed classifications of ~ 3000 SDSS galaxies suggests that these

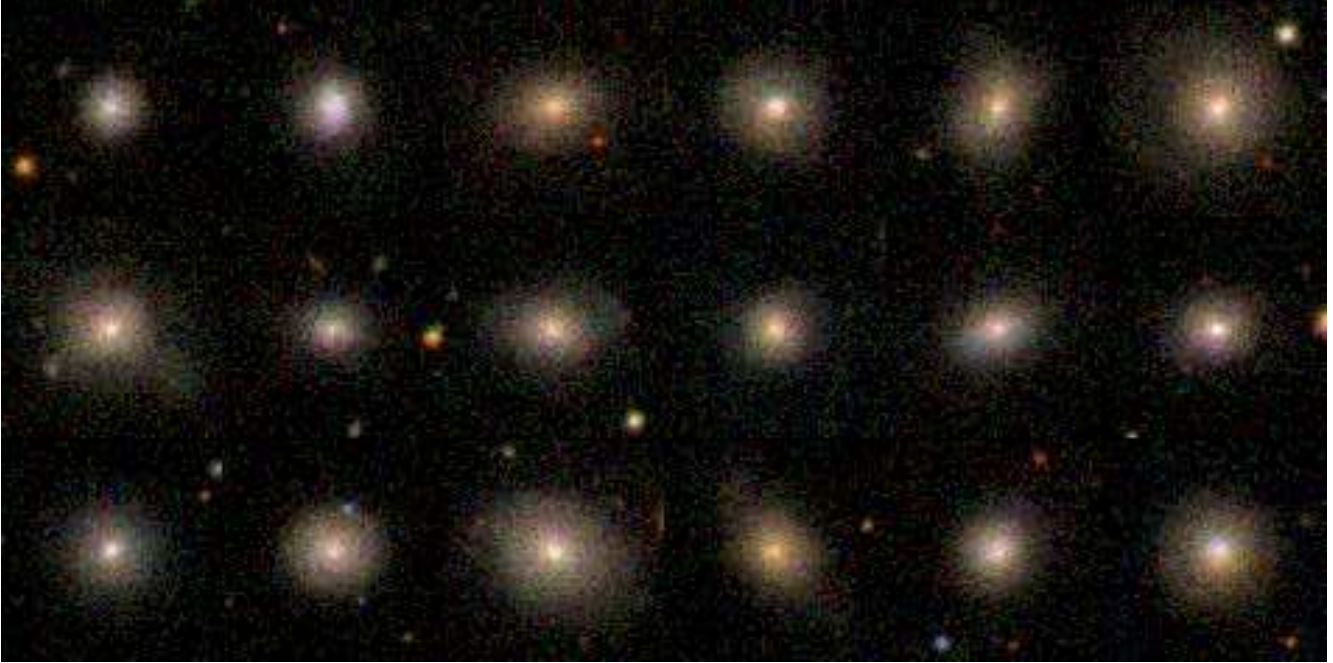


Figure 4. In this Figure, we show example SDSS *gri* composite colour images for a sample of blue early-type galaxies. The galaxies shown here are all classified as purely starforming (see Section 2.4). The objects here all have aperture-corrected $H\alpha$ SFR $> 5 M_{\odot}\text{yr}^{-1}$. These objects all have higher star formation rates than any previously known visually-classified early-type galaxy. The images measure $51.2'' \times 51.2''$.

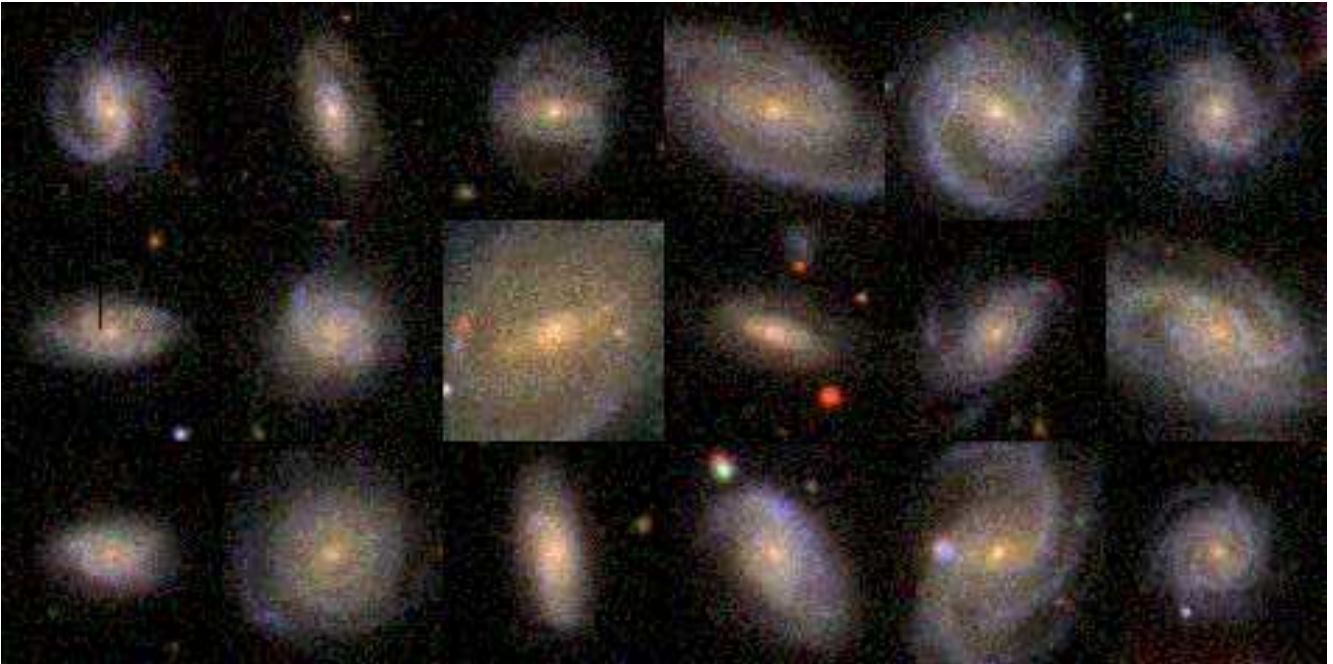


Figure 5. In this Figure, we show example SDSS *gri* composite colour images for a sample of face-on spiral galaxies selected by applying the same redshift and luminosity cuts that define our blue early-type galaxy sample. Their purpose is to indicate the image quality in Figure 4, which may not be apparent due to the lack of features of early-type galaxies. These images also indicate how a starforming disk or spiral arms of any prominence appear in images of this quality and so establishes their absence in our morphological early-type sample.

extra galaxies are likely to be S0 galaxies. Each of the galaxies included in the present sample were inspected by an expert classifier (KS) and found to be of early-type morphology.

A further advantage of the Galaxy Zoo classifications rests in the fact that we have multiple classifications for every object.

This allows us to statistically analyse the distribution of classifications to assess its reliability. In a companion paper, Bamford et al. (2008) statistically assess the bias of galaxy classifications from Galaxy Zoo and SDSS as function of luminosity and redshift. This study underlines the need for our selection of low redshift, high-

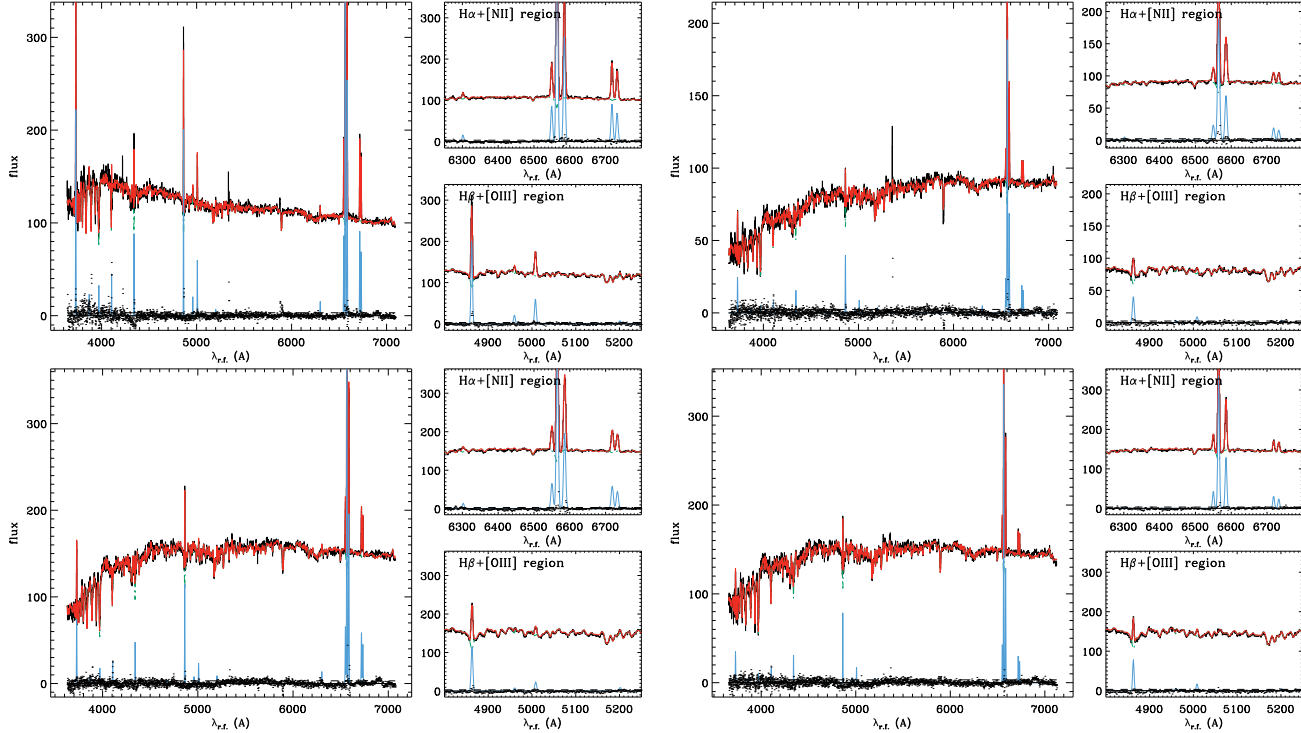


Figure 6. We show the SDSS spectra of four blue early-type galaxies processed with GANDALF. For each galaxy, we show the whole galaxy spectrum in the restframe. The best fit is overplotted in red, while the fit to the emission lines is shown in blue. The residuals for this fit are also shown by the small points at the lower end of each panel, where the dashed lines further show the average level of the residuals that is used to assess the detection of the emission lines. We further focus in on two wavelength regions of interest around $H\alpha+[NII]$ and $H\beta+[OIII]$. All four spectra feature deep Balmer absorption lines and some show considerable dust extinction.

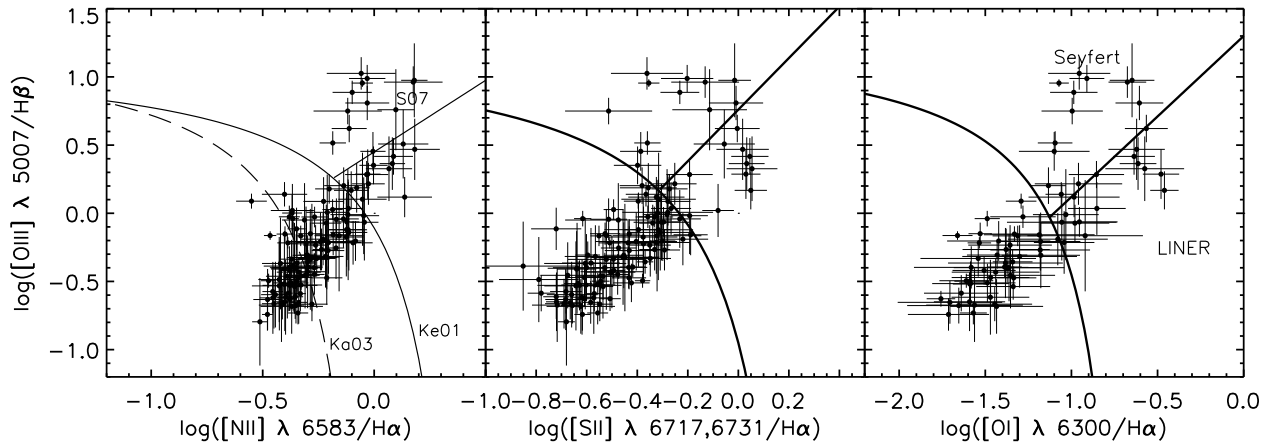


Figure 7. In this Figure, we show the emission line ratio diagrams for our blue early-type galaxy sample (BPT diagram; Baldwin, Phillips, & Terlevich 1981). Only objects where all four lines in each diagram are detected with $S/N > 3$ are plotted. In each panel, we use a different line from left to right: $[NII] \lambda 6583$, $[SII] \lambda 6583$ and $[OI] \lambda 6583$. All objects below the line labelled Ka03 (Kauffmann et al. 2003) are classified as purely starforming. All objects between the Ka03 line and the line labelled Ke01 (Kewley et al. 2001) are AGN+SF composites. The line from S07 divides Seyferts and LINERS on the $[NII]$ diagram. All objects beyond this line are separated into Seyfert AGN and LINERs where possible with the $[OI]$ or $[SII]$ diagrams.

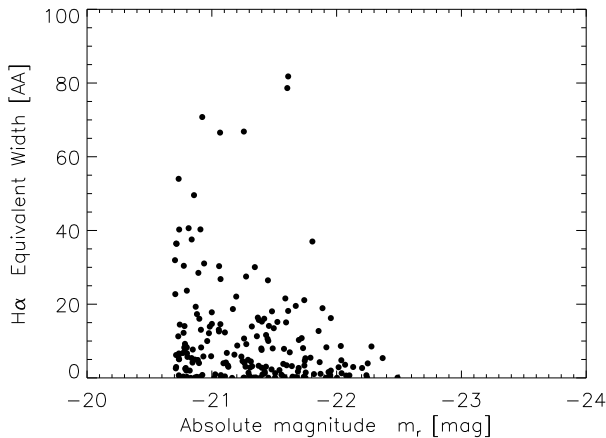
luminosity galaxies for obtaining the high reliability of visual inspection needed to rule out any significant late-type/spiral interlopers in this sample. Based on the estimates of Bamford et al. (2008), we conclude that our sample as a maximum contamination of spiral interlopers of $\sim 4\%$, which corresponds to 8 objects in the blue early-type sample. This makes our sample exceedingly clean; Sa

spiral galaxies with distinct disks and spiral arms are *not* contributing to our sample. We confirm this by visually inspecting all 204 objects.

Table 1. Emission Line Classification Results for blue early-type galaxies

Classification	Number	Fraction Galaxies
Blue early-type galaxies	204	100%
Starforming	50	24.5%
AGN-SF composite	52	25.5%
Seyfert	15	7.4%
LINER	11	5.4%
Weak emission lines ¹	76	37.3%

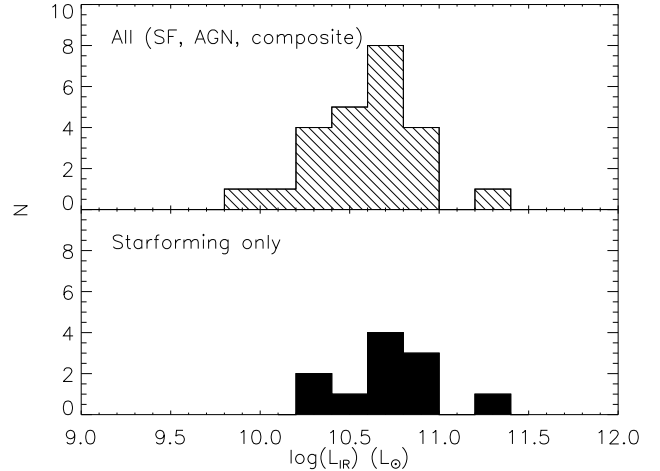
¹ Measurement of at least one of $H\alpha$, $H\beta$, [NII] and [OIII] has signal-to-noise less than 3; see Section 2.4.

**Figure 8.** The $H\alpha$ equivalent width as a function of galaxy absolute magnitude to give an indication of the emission line strength.

2.4 Emission Line Measurement

Optical emission lines are a well-established and powerful tool for identifying and separating starforming galaxies from AGN (Baldwin et al. 1981; Veilleux & Osterbrock 1987). We measure the optical emission lines of our blue early-type galaxy sample using the GANDALF package¹ (Sarzi et al. 2006). In Figure 6 we show four example spectra of blue early-type galaxies processed with GANDALF. We use the main emission lines ([OIII] λ 5007, $H\beta$, $H\alpha$, [NII] λ 6583, [SII] λ 6583, [OI] λ 6583) measured from such processed spectra on diagnostic diagrams (Kauffmann et al. 2003; Miller et al. 2003; Kewley et al. 2001, 2006). We classify all galaxies where the measurements of $H\alpha$, $H\beta$, [NII] and [OIII] have a signal-to-noise of at least 3 and divide them into purely starforming, SF-AGN composites and AGN (Seyfert or LINER by comparing their line ratios on a BPT diagram). Where available, we use the [OI] diagram for the Seyfert-LINER separation. If [OI] is unavailable, then we use [SII] and if that also is not available, the [NII] diagram. To give an idea of the emission line strength, we plot the $H\alpha$ equivalent width as a function of galaxy luminosity in Figure 8.

In Figure 7 and Table 1, we show our results. Only 25% of the blue early-type galaxies are unambiguously classified as actively

**Figure 9.** The distribution of infrared luminosities L_{IR} for our blue early-type galaxy sample. The top panel is for the entire blue early-type galaxy sample, while the bottom shows the starforming objects only. The L_{IR} of all objects may in part be due an AGN contribution, while the purely starforming sample is likely infrared luminous mostly due to star formation.

starforming (corresponding to 1.5% of the entire early-type galaxy population).

Interestingly, we find that 37% of blue early-type galaxies do not have $S/N > 3$ in at least one of the four lines. We call this class ‘weak emission line’ galaxies. The lines most likely to drop below $S/N = 3$ are $H\beta$ and [OIII]. Out of the 76 galaxies classified as quiescent, 32 have three lines out of four lines. This lack of emission lines means that those galaxies may be no longer strongly starforming or may not be host to a powerful AGN and that the source of ionising radiation driving the emission lines is weak.

It is possible to determine an upper limit on the current SFR of our unclassifiable blue early-type galaxies by using whatever $H\alpha$ line flux is measured by GANDALF. We find that they have SFRs $< 1 M_{\odot}\text{yr}^{-1}$; this represents the low-SFR tail of the sample (see Section 3.1). S07 found that blue early-type galaxies typically undergo a burst in which 1-10% of their stellar mass are formed on a timescale of ~ 100 Myr. These blue early-type galaxies without emission lines may represent the passive evolutionary phase which follows this burst of star formation. They may represent the population of early-types where the suppression of star formation is complete and they are rapidly moving towards the red sequence (S07). They may be distinct from normal passive early-type galaxies in their UV/optical colours as demonstrated by Yi et al. (2005). Kriek et al. (2006, 2007) discuss a potentially similar sample of early-type galaxies with suppressed star formation at high redshift.

3 THE PROPERTIES OF BLUE EARLY-TYPE GALAXIES

We now discuss the properties of the blue early-type galaxy population in detail. We note that in our discussion of star formation, we *only* refer to those blue early-type galaxies classified as purely starforming on the emission line diagrams (see Section 2.4).

¹ Available at: <http://www.strw.leidenuniv.nl/sauron/>

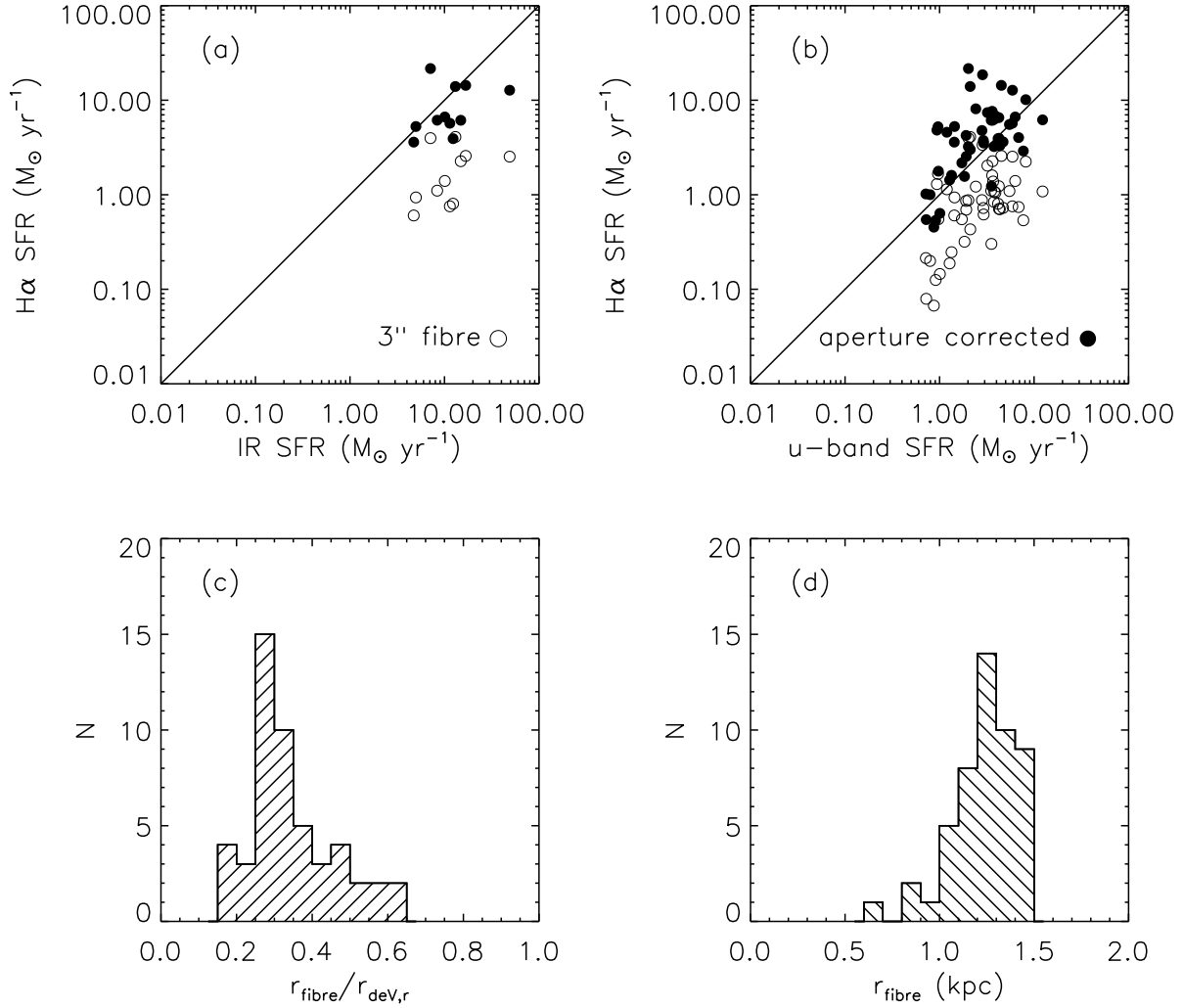


Figure 10. In panels (a) and (b), we compare our various SFR indicators against each other for those blue early-type galaxies classified as purely starforming. In each, the empty circles stand for the 3'' fibre aperture H α SFR, while the filled circles represent the aperture-corrected H α SFR. In (a), we compare these two to the IR SFR and in (b) to the u -band SFR. We also indicate the line of the 1:1 correspondence. In the case of panel (a), we find that the 3'' fibre SFR is systematically offset from the *total* IR SFR, while the aperture-corrected SFR gives a good match. In the case of panel (b), the 3'' fibre SFR again is systematically lower than the u -band SFR, while the aperture-corrected SFR is systematically higher. From this comparison, we conclude that while neither 3'' fibre nor aperture-corrected SFR is perfect, the aperture-corrected SFR is closer to the IR SFR. In panel (c), we show the histogram of the ratio of the 3'' fibre to the de Vaucouleurs scale radius and in (d), we show the histogram of physical radii in kpc that the 3'' fibre corresponds to.

3.1 Infrared Luminosities and Star Formation Rates

We match our blue early-type galaxy sample to the *IRAS* (*Infrared Astronomical Satellite*) Faint Source Catalog v.2 (Moshir et al. 1990) to measure their infrared luminosities L_{IR} (Sanders & Mirabel 1996), yielding 24 matches. We find that all but two of those early-type galaxies that are detected range between $10^{10} < L_{\text{IR}} < 10^{11} L_{\odot}$ and two objects are above the limit of luminous infrared galaxies (LIRGs; $L_{\text{IR}} > 10^{11} L_{\odot}$). In Figure 9, we plot the distribution of infrared luminosities split into purely starforming blue early-types and everything else. We calculate IR (infra-red) SFRs for those galaxies in our sample that have been detected by IRAS using the calibration of Gao & Solomon (2004) and find that the IR SFRs range between $5 < \text{SFR} < 50 M_{\odot} \text{ yr}^{-1}$. Using the relationships of Gao & Solomon (2004),

we can also estimate the range of HCN luminosity ($10^7 < L_{\text{HCN}} < 10^8 \text{ K km s}^{-1} \text{ pc}^2$) and CO luminosity ($10^{8.5} < L_{\text{CO}} < 10^{9.5} \text{ K km s}^{-1} \text{ pc}^2$). The IRAS FSC has a very shallow flux limit, so that any detections are due to the most luminous and nearest objects. In order to study the population as a whole, we turn to H α as a tracer of the SFR.

3.2 Star Formation Rates

We measure the H α line luminosity, correcting for internal extinction based on the Balmer decrement, and compute the star formation rate using the calibration of Kennicutt (1998) for our purely starforming blue early-type sample. We ignore the AGN+SF composites, as we cannot know what fraction of the H α derives from star formation. Since SDSS spectroscopic fibres have a 3'' diameter,

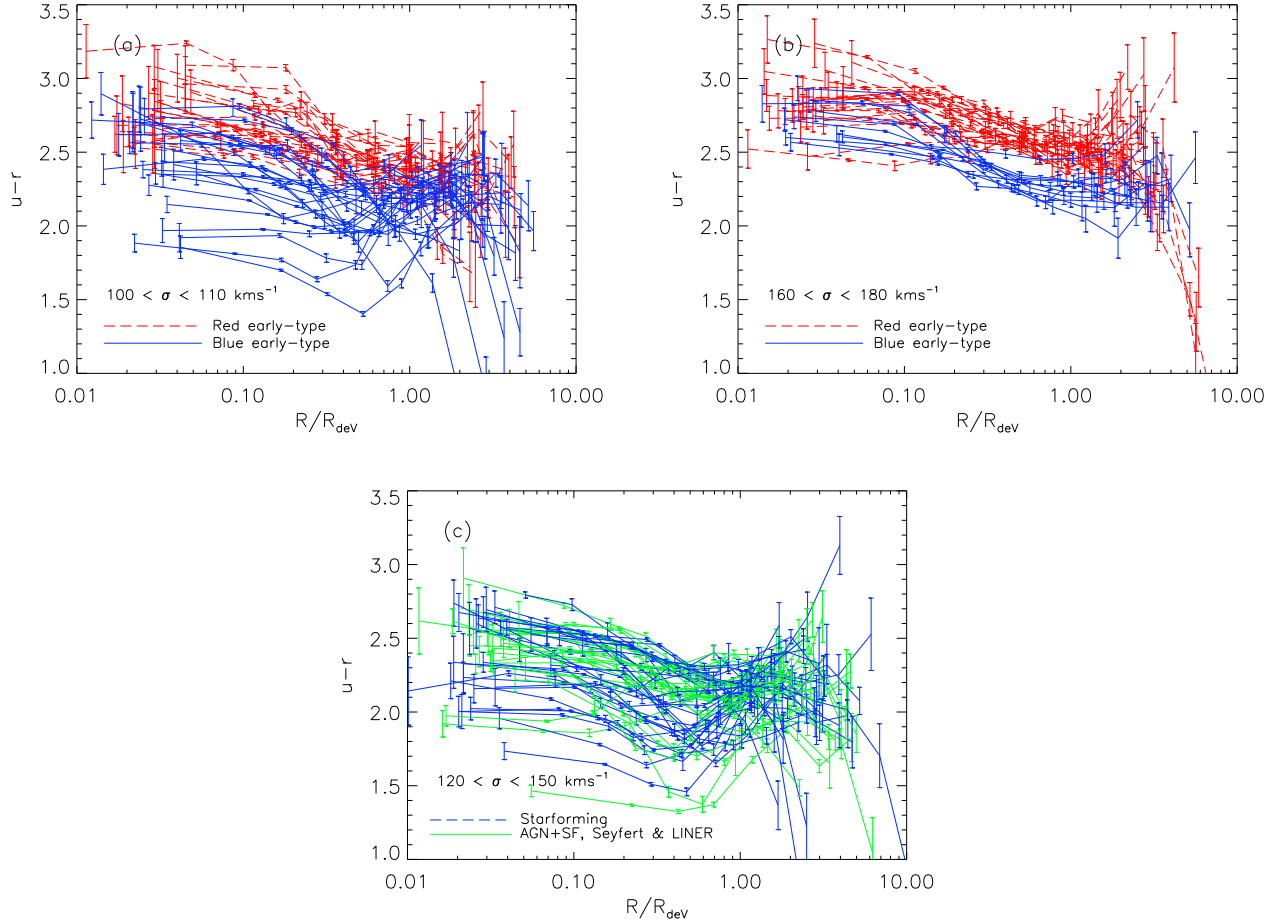


Figure 11. The $u - r$ colour profiles of blue and red early-type galaxies. The radial distance is normalised to the de Vaucouleurs scale radius derived by the SDSS photometric pipeline. In panels a and b, we show the colour profiles of blue and red early-types in two velocity dispersion bins. In both cases, we find that the blue colours extend to at least the scale radius, supporting the idea that the star formation in this population is spatially extended. In panel c) we test whether there is any clear systematic difference in the colour profile between the purely starforming early-types (in blue), and those showing evidence for an AGN in the emission lines (AGN+SF, Seyfert and LINER; in green).

this yields the SFR in the central $3''$ of the galaxy, which corresponds for this sample to a mean of 2 kpc in radius. Assuming that the distribution of the star formation follows the stellar light of the galaxy, we can estimate the $H\alpha$ luminosity lost outside the fibre from the ratio of the r -band flux within the $3''$ and the total Petrosian r -band flux. This typically scales the light from $\sim 20\%$ inside the fibre to 100%. In order to determine whether this aperture correction is appropriate, we compare with independent tracers of the total SFR: the IR SFR from the *IRAS* observations and the SFR from the u -band light (Hopkins et al. 2003), corrected for extinction using the Balmer decrement. Our galaxies are effectively point sources for *IRAS* and so include emission from the entire galaxy.

In Figure 10, we show the comparison between our SFR indicators. While there is significant scatter, the aperture corrected SFR is generally in better agreement with the IR SFR than the fibre SFR and the u -band SFR lies between the aperture-corrected and fibre SFR. This means that the central fibre SFR only samples a fraction of the total SFR, which implies that star formation in blue early-type galaxies is not confined to a central disk or nuclear starburst, but extends over the entire galaxy (see also Sarzi et al. 2006).

Even with the correction, there is still an offset between the

$H\alpha$ and u -band SFRs. This may be due to the fact that the u -band does not probe sufficiently obscured SF, while the IR does. This underestimation of the SFR by the u -band light is thus unsurprising. The better agreement between aperture-corrected $H\alpha$ and IR SFR argues that $H\alpha$ suffers less from this effect.

For the remainder, we use the aperture-corrected $H\alpha$ SFR which is available for the entire starforming sample, unlike the IR SFR.

3.3 Colour Profiles

Another way to probe the distribution of young stars in our galaxies is to plot the $u - r$ colour as a function of radius. In Figure 11, we plot the $u - r$ radial profiles for blue and red early-types in two velocity dispersion bins. Comparing at the same velocity dispersion is important, but at low velocity dispersions, it can be challenging (c.f. Section 2.2). At low velocity dispersions, most passive, red early-types are not included in our volume limited sample with a bias against the redder, less luminous objects. We nevertheless plot the colour profiles for a sample with $100 < \sigma < 110 \text{ km s}^{-1}$ (Fig. 11a) and for $160 < \sigma < 180 \text{ km s}^{-1}$ (Fig. 11b). In both

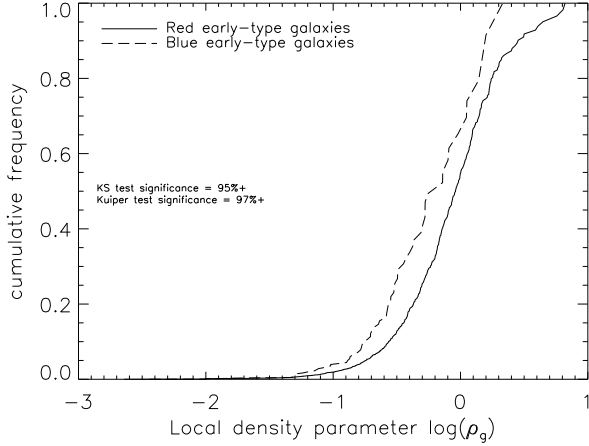


Figure 12. We show cumulative frequency distribution of the local density parameter $\log(\rho_g)$ (see Schawinski et al. 2007a) for both blue early-type galaxies and their red counterparts in the same velocity dispersion regime ($110 < \sigma < 150 \text{ km s}^{-1}$ in order to avoid selection bias with mass. We use both a KS and a Kuiper test to assess the significance of the different distributions and find that they are different at 95% and 97% significance, respectively. Blue early-type galaxies prefer lower density environments compared to their red counterparts.

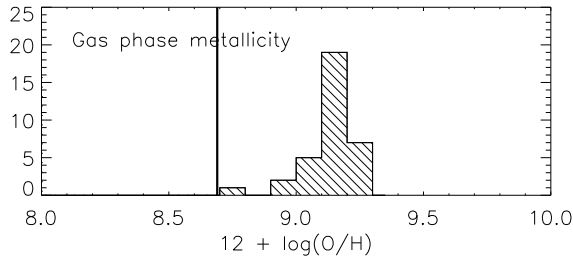


Figure 13. This Figure shows the gas phase metallicity of the starforming early-types from the catalog of Tremonti et al. (2004). The vertical line indicates the solar value (Allende Prieto et al. 2001).

cases, we find that the $u - r$ colour is significantly bluer out to at least the effective radius, supporting our finding that the star formation is extended, rather than circumnuclear, as has been found for some massive radio galaxies (Aretxaga et al. 2001; Holt et al. 2007). Some blue early-types do become redder at about R_{dev} , others remain blue out to several radii. Some of the massive blue early-types in Figure 11b tend to red $u - r$ colour within the central $1/10 R_{\text{dev}}$; this may be due to high levels of extinction.

We also test whether there is any clear difference between the purely starforming blue early-type galaxies and those with any evidence for AGN activity (i.e. AGN+SF, Seyfert and LINER). We plot the colour profiles in Figure 11c and conclude that there is no clear trend apparent.

3.4 Gas Phase Metallicities

The chemical enrichment of the interstellar medium (ISM) of galaxies is an important probe of their chemical evolution. In order

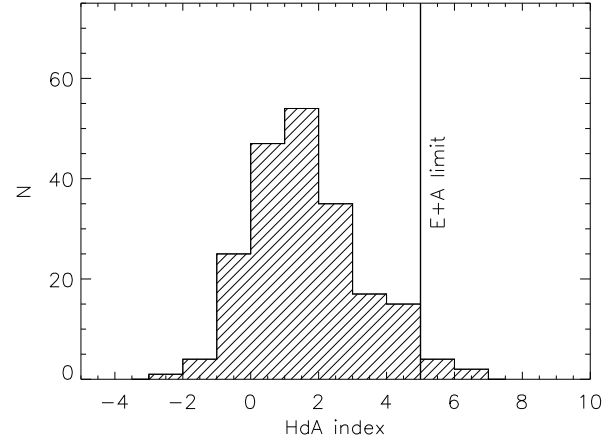


Figure 14. Histogram of the H δ A line index for the blue early-type galaxy sample. We indicate the E+A galaxy limit of 5\AA .

to place blue early-type galaxies in context, we obtain gas phase metallicities from the SDSS catalogue of Tremonti et al. (2004) for those blue early-type galaxies classified as purely starforming. We show the distribution of gas-phase metallicities for those objects with matches in their catalogue in Figure 13 (Tremonti et al. 2004). We find that the gas phase metallicities are all supersolar (adopting the solar value of Allende Prieto et al. 2001).

From the BPT diagrams in Figure 7, we can see that there is a lack of objects with high $[\text{OIII}]/\text{H}\beta$ ratios on the starforming locus is naturally accounted for by the lack of low metallicity gas in blue early-types. Comparing to the observed mass-metallicity relation of Tremonti et al. (2004), the gas phase metallicities of blue early-type galaxies are as expected and the high metallicities are a result of our luminosity cut.

3.5 Environment

The effect of environment on galaxy formation has seen vigorous debate since the discovery of Oemler (1974) and Dressler (1980) that early-type galaxies preferentially reside in clusters. It is not clear whether in particular the scaling relations of the stellar populations of early-type galaxies vary at all with environment. We measure the local density of our sample using the environment parameter ρ_g defined by Schawinski et al. (2007a) (see also Yoon et al. 2008). This parameter samples the local galaxy distribution with a Gaussian kernel of 2 Mpc and represents a weighted local number density. We calculate ρ_g for our blue early-type galaxy sample and for the corresponding red early-type galaxies and show the resulting cumulative distributions in Figure 12. In order to avoid bias with galaxy mass, we limit both the blue and red early-type sample to a range of $110 < \sigma < 150 \text{ km s}^{-1}$.

The results for the two distributions of ρ_g show that blue early-type galaxies clearly reside in lower-density environments compared to their red counterparts at the same velocity dispersion. We perform a KS test and find a probability of the two distributions being drawn from different parent distributions of 95%. For a Kuiper test, the significance is 97%. In fact, blue early-type galaxies appear to be virtually absent at the typical densities of cluster centres as defined by a commonly used cluster catalogue based on SDSS, the

C4 cluster catalogue of Miller et al. (2005) which were explored by Schawinski et al. (2007a).

4 DISCUSSION

Blue early-type galaxies represent a fascinating phase in the evolution of galaxies. Quite what place they take in the overarching picture is still unclear. There are three general scenarios that might account for them. They could represent the result of a spiral-spiral merger whose end-product will eventually join the red sequence in passive evolution. They might also be early-type galaxies on the red sequence that are undergoing an episode of star formation due to the sudden availability of cold gas, making them leave the red sequence before rejoining it. The third possibility is that they are mixed early-type/late-type mergers (e.g. Khochfar & Burkert 2003), meaning that one progenitor originates from each the blue cloud and the red sequence. Which of these scenarios – or which combination thereof – is occurring here is unclear. We provide Table 2 to enable follow-up observations of these objects to further illuminate their nature.

4.1 Are there any Nearby Counterparts?

In the nearby Universe, our SDSS blue star-forming early-type galaxies could correspond to objects like NGC 3032, which is the bluest of the early-type galaxies observed in the course of the SAURON integral-field survey (de Zeeuw et al. 2002) and the one showing by far the strongest nebular emission (Sarzi et al. 2006). NGC 3032 is also unique in that it shows star formation across the entire SAURON field-of-view (corresponding to approximately one effective radius), whereas in early-type galaxies with lower levels of star formation, this occurs in circumnuclear rings. The equivalent width of the integrated nebular emission of NGC 3032 (4\AA within one effective radius for $H\beta$) is also sufficiently strong that it would have been detected by SDSS observations and end up as being classified as one of our star-forming blue early-type galaxies.

Arguing from population statistics, that only one such a galaxy is found among the 48 objects surveyed by SAURON is also consistent with the 1.5% fraction of the early-type population that we found to be blue and star-forming.

4.2 Comparison to Theoretical Models

We now explore the blue early-type galaxy population in simulations of galaxy formation.

4.2.1 Semi-Analytic Models

In order to compare our results with the predictions of the Λ CDM paradigm we use semi-analytical modelling (SAM) (Khochfar & Burkert 2005; Khochfar & Silk 2006) including an empirical description for AGN-feedback (Schawinski et al. 2006). This model reproduces well the fraction of NUV-blue early-type galaxies as a function of magnitude and velocity dispersion (Schawinski et al. 2006). It should be noted that without our AGN-feedback prescription almost all of the simulated early-type galaxies were blue in the luminosity range of interest; reproducing the colours of early-type galaxies remains a difficult challenge for SAMs. We here compare the range of star formation rates for the blue early-type population with those obtained from the observations.

Adopting a magnitude limit of $M_r = -21$ and the same 3σ cut in $u - r$ as described above to select blue early-type galaxies, we find that 7.7% of model early-type galaxies are selected as blue. This fraction is comparable to the $5.7 \pm 0.4\%$ that we observe (see Figure 1); the difference may be due to massive gas-rich mergers that are considered bulge-dominated objects in the model, but may have sufficiently disturbed morphologies to have been classified as mergers in Galaxy Zoo. In the blue early-type galaxies in the model, we find SFRs ranging from $0.1 - 45 M_{\odot}\text{yr}^{-1}$, with a strong peak around $1 M_{\odot}\text{yr}^{-1}$ and an extended tail to the upper end of the SFR range. The fraction of blue early-type galaxies showing SFR above $1 M_{\odot}\text{yr}^{-1}$ is $\sim 45\%$ and as such is larger than the above reported 25%. However, the combined starforming and AGN-SF composite population accounts for $\sim 50\%$ of the galaxies and is well above the fraction of starforming early-types in the SAM, indicating that a large fraction of the AGN-SF composite population might indeed be starforming.

4.2.2 A Merger Trigger for Blue Early-types?

Kaviraj et al. (2007b) have performed numerical simulations of minor mergers to determine their role in the recent star formation histories of early-type galaxies and explore whether satellite accretion could produce the blue UV colours that seem to be common amongst the low redshift early-type population (Yi et al. 2005; Schawinski et al. 2007a; Kaviraj et al. 2007c). The peak SFRs produced in minor mergers (with mass ratios of 1:6 and a satellite with a gas fraction of 20%) is less than $\sim 1 M_{\odot}\text{yr}^{-1}$ (see their Figure 1). Even if larger mass ratios (e.g. 1:4) and more gas-rich satellites (e.g. with gas fractions of 40%) are considered the peak SFRs in these events are unlikely to be higher than a few $M_{\odot}\text{yr}^{-1}$. Therefore, it is unlikely that the star formation activity observed in our sample is triggered by minor mergers.

Accretion of cold gas from the halo should be negligible if feedback processes efficiently maintain the temperature of the hot gas reservoir in early-type galaxies (Binney 2004), but it cannot be ruled out. A plausible route for the triggering of the star formation we are witnessing in these blue early-type systems is gas-rich major mergers, where at least one of the progenitors is a late-type galaxy. Such events are predicted by current semi-analytic models (Khochfar & Burkert 2003; Kaviraj et al. 2006) and so may be a natural trigger for the the time sequence of S07.

4.3 Are Blue Early-type Galaxies Progenitors of E+A Galaxies?

An intriguing possibility worth discussing here is that the blue early-type galaxy population may be at least partially linked to the E+A galaxy phenomenon via an evolutionary sequence. E+A (or k+a) galaxies have spectra undergoing no ongoing star formation indicated by a lack of $H\alpha$ and [OII] emission lines but indicating a recent past starburst resulting in a considerable mass-fraction in intermediate age stars (the ‘A’ in E+A denotes A stars). First noted by Dressler & Gunn (1983), E+A galaxies are rare and seem to reside mostly in low-density environment and their deep Balmer lines together with their UV-optical colours point to a pathway in which star formation was truncated on short timescales (Kaviraj et al. 2007a).

The usual selection of E+A galaxies is via a rejection of spectra with signs of active star formation and extremely deep Balmer lines. If we ignore the star formation criteria and simply focus on

the Balmer line cut, only a small fraction of blue early-type galaxies (6/204, 2.9%, see Figure 14) would meet the $H\delta A > 5\text{\AA}$ criterion. However, blue early-types are still actively starforming resulting in smaller typical $H\delta A$ equivalent widths (EW); the $H\delta A$ EW peaks at intermediate ages. Thus, it is conceivable that if star formation is suddenly suppressed (e.g. via AGN feedback, S07 and Schawinski et al. 2009a,b), then a part of the blue early-type galaxy population may represent the progenitors of E+A galaxies. The deep Balmer lines apparent in the spectra of blue early-types (see Figure 6) indicate that a substantial intermediate-age population may be present.

5 CONCLUSIONS

In this Paper, we investigate a volume-limited sample of visually identified early-type galaxies selected from Galaxy Zoo and SDSS DR6. Our selection via morphology only has allowed us to study the population of *optically blue* early-type galaxies that do not reside on the red sequence like their passive counterparts. We determine the number fraction of these blue early-types and discuss selection effects. The most prominent caveat is the fact that absolute magnitudes can be boosted significantly, giving the impression that blue early-type galaxies are massive. However, their velocity dispersions are moderate and extremely few exceed 200 km s^{-1} , implying masses below $10^{11} M_{\odot}$. There are almost no **massive** blue early-type galaxies in the low redshift Universe. We show that the young stellar populations present in blue early-type galaxies cause them to scatter off the Faber-Jackson relation and using simple fading/ageing models determine that they can fade back onto the Faber-Jackson relation within $\sim 1 \text{ Gyr}$ for small young mass fractions of a few percent.

We use emission line diagnostic diagrams to classify them into purely starforming (25%), SF+AGN composites (25%) and AGN (12%). The remaining blue early-type galaxies show no strong emission lines and so have suppressed their star formation and show no AGN (as discussed in S07). We discuss a possible connection between these objects and E+A/K+A galaxies in Section 4.3.

Using a variety of measures ($H\alpha$, u -band and IR), we determine the range of star formation rates in blue early-type galaxies and find a wide range from $0.5 < \text{SFR} < 50 M_{\odot} \text{ yr}^{-1}$. The higher values are the highest values reported for low redshift early-type galaxies. By comparing the star formation rate probed by the central SDSS $3''$ fibres to total IR star formation rates, we conclude that the star formation in starforming blue early-type galaxies is not confined to a central circumnuclear starburst, but extends spatially across most of the galaxy. We independently confirm this by verifying that the radial colour profiles exhibit blue colours out to at least the de Vaucouleurs scale radius, and in some cases, beyond. We also measure the gas phase metallicity and find them to be supersolar in every case, consistent with the mass-metallicity relation of Tremonti et al. (2004).

We measure the local environment using the measure of Schawinski et al. (2007a) and Yoon et al. (2008) and find, at a given velocity dispersion, a statistically significant difference between red and blue early-type galaxies. Blue early-type galaxies are less frequent at the highest densities compared to their red counterparts at the same mass, implying a role of environment.

We discuss the place of these objects in our current understanding of galaxy formation. A comparison to numerical simulation of minor mergers suggests that minor mergers are an unlikely

trigger mechanism; this leaves major mergers (either early-early or early-late) and major cooling events in red early-type galaxies as plausible triggers. Further observations of blue early-type galaxies should be able to resolve this. Deep optical imaging should reveal tidal tails and other features if they are the result of major mergers (c.f. van Dokkum 2005).

In order to allow the further study of this exciting population, we provide a catalog of all blue early-type galaxies presented in this paper in Table 2.

6 ACKNOWLEDGEMENTS

We would like to thank Adrienne Slyz and Julien Devriert for helpful comments and suggestions. We also would like to thank Alice Sheppard and Edd Edmondson for their help in administering the Galaxy Zoo forum. KS is supported by the Henry Skynner Junior Research Fellowship at Balliol College Oxford. CJL acknowledges support from the STFC Science in Society Programme. S. Kaviraj acknowledges a Leverhulme Early-Career Fellowship, a BIPAC fellowship and a Research Fellowship from Worcester College, Oxford. This work was supported by grant No. R01-2006-000-10716-0 from the Basic Research Program of the Korea Science and Engineering Foundation to SKY.

Funding for the SDSS and SDSS-II has been provided by the Alfred P. Sloan Foundation, the Participating Institutions, the National Science Foundation, the U.S. Department of Energy, the National Aeronautics and Space Administration, the Japanese Monbukagakusho, the Max Planck Society, and the Higher Education Funding Council for England. The SDSS Web Site is <http://www.sdss.org/>.

The SDSS is managed by the Astrophysical Research Consortium for the Participating Institutions. The Participating Institutions are the American Museum of Natural History, Astrophysical Institute Potsdam, University of Basel, University of Cambridge, Case Western Reserve University, University of Chicago, Drexel University, Fermilab, the Institute for Advanced Study, the Japan Participation Group, Johns Hopkins University, the Joint Institute for Nuclear Astrophysics, the Kavli Institute for Particle Astrophysics and Cosmology, the Korean Scientist Group, the Chinese Academy of Sciences (LAMOST), Los Alamos National Laboratory, the Max-Planck-Institute for Astronomy (MPIA), the Max-Planck-Institute for Astrophysics (MPA), New Mexico State University, Ohio State University, University of Pittsburgh, University of Portsmouth, Princeton University, the United States Naval Observatory, and the University of Washington.

REFERENCES

- Adelman-McCarthy J. K. et al. 2008, ApJS, 175, 297
- Allende Prieto C., Lambert D. L., Asplund M., 2001, ApJ, 556, L63
- Aretxaga I., Terlevich E., Terlevich R. J., Cotter G., Díaz Á. I., 2001, MNRAS, 325, 636
- Baldry I. K., Glazebrook K., Brinkmann J., Ivezić Ž., Lupton R. H., Nichol R. C., Szalay A. S., 2004, ApJ, 600, 681
- Baldwin J. A., Phillips M. M., Terlevich R., 1981, PASP, 93, 5
- Bamford S. P. et al. 2008, ArXiv e-prints, arXiv:0805.2612
- Bernardi M. et al. 2003, AJ, 125, 1849
- Bernardi M., Sheth R. K., Nichol R. C., Schneider D. P., Brinkmann J., 2005, AJ, 129, 61

- Bettoni D., Buson L. M., 1987, *AAPS*, 67, 341
 Binney J., 2004, *MNRAS*, 347, 1093
 Bower R. G., Lucey J. R., Ellis R. S., 1992, *MNRAS*, 254, 601
 Calzetti D., Armus L., Bohlin R. C., Kinney A. L., Koornneef J.,
 Storchi-Bergmann T., 2000, *ApJ*, 533, 682
 Chester C., Roberts M. S., 1964, *AJ*, 69, 635
 Constantin A., Hoyle F., Vogeley M. S., 2008, *ApJ*, 673, 715
 de Zeeuw P. T. et al. 2002, *MNRAS*, 329, 513
 Doublier V., Comte G., Petrosian A., Surace C., Turatto M., 1997,
AAPS, 124, 405
 Dressler A., 1980, *ApJ*, 236, 351
 Dressler A., Gunn J. E., 1983, *ApJ*, 270, 7
 Driver S. P. et al. 2006, *MNRAS*, 368, 414
 Faber S. M., Jackson R. E., 1976, *ApJ*, 204, 668
 Faber S. M. et al. 2007, *ApJ*, 665, 265
 Fukugita M. et al. 2007, *AJ*, 134, 579
 Fukugita M., Nakamura O., Turner E. L., Helmboldt J., Nichol
 R. C., 2004, *ApJ*, 601, L127
 Gao Y., Solomon P. M., 2004, *ApJ*, 606, 271
 Graves G. J., Faber S. M., Schiavon R. P., Yan R., 2007, *ApJ*, 671,
 243
 Holt J., Tadhunter C. N., González Delgado R. M., Inskip K. J.,
 Rodríguez J., Emonts B. H. C., Morganti R., Wills K. A., 2007,
MNRAS, 381, 611
 Hopkins A. M. et al. 2003, *ApJ*, 599, 971
 Huchra J. P., 1977a, PhD thesis, AA(CALIFORNIA INSTITUTE
 OF TECHNOLOGY.)
 Huchra, J. P. 1977b, *ApJS*, 35, 171
 Kauffmann G. et al. 2003, *MNRAS*, 346, 1055
 Kaviraj, S., Devriendt, J. E. G., Ferreras, I., Yi, S. K., & Silk, J.
 2006, arXiv:astro-ph/0602347
 Kaviraj S., Kirkby L. A., Silk J., Sarzi M., 2007a, *MNRAS*, 382,
 960
 Kaviraj S., Peirani S., Khochfar S., Silk J., Kay S., 2007b, ArXiv
 e-prints, arXiv:0711.1493
 Kaviraj S. et al. 2007c, *ApJS*, 173, 619
 Kennicutt Jr. R. C., 1998, *ApJ*, 498, 541
 Kewley L. J., Dopita M. A., Sutherland R. S., Heisler C. A.,
 Trevena J., 2001, *ApJ*, 556, 121
 Kewley L. J., Groves B., Kauffmann G., Heckman T., 2006, *MN-*
RAS, 372, 961
 Khochfar S., Burkert A., 2003, *ApJ*, 597, L117
 —, 2005, *MNRAS*, 359, 1379
 Khochfar S., Silk J., 2006, *MNRAS*, 370, 902
 Kriek M. et al. 2007, *ApJ*, 669, 776
 Kriek M. et al. 2006, *ApJ*, 649, L71
 Kunth D., Maurogordato S., Vigroux L., 1988, *A&A*, 204, 10
 Lintott C. J. et al. 2008, *MNRAS*, 389, 1179
 Maraston C., 2005, *MNRAS*, 362, 799
 Miller C. J., Nichol R. C., Gómez P. L., Hopkins A. M., Bernardi
 M., 2003, *ApJ*, 597, 142
 Miller C. J. et al. 2005, *AJ*, 130, 968
 Moshir M. et al. 1990, in *Bulletin of the American Astronomical*
Society, Vol. 22, *Bulletin of the American Astronomical Society*,
 pp. 1325–+
 Nelan J. E. et al. 2005, *ApJ*, 632, 137
 Oemler A. J., 1974, *ApJ*, 194, 1
 Salim S. et al. 2007, *ApJS*, 173, 267
 Sanders D. B., Mirabel I. F., 1996, *ARA&A*, 34, 749
 Sarzi M. et al. 2006, *MNRAS*, 366, 1151
 Schawinski K. et al. 2007a, *ApJS*, 173, 512
 Schawinski K. et al. 2006, *Nature*, 442, 888
 Schawinski K., Thomas D., Sarzi M., Maraston C., Kaviraj S., Joo
 S.-J., Yi S. K., Silk J., 2007b, *MNRAS*, 382, 1415
 Schawinski, K., et al. 2009a, *ApJ*, 690, 1672
 Schawinski, K., Virani, S., Simmons, B., Urry, C. M., Treis-
 ter, E., Kaviraj, S., & Kushkuley, B. 2009b, *ApJL*, in press,
 arXiv:0901.1663
 Telles E., Melnick J., Terlevich R., 1997, *MNRAS*, 288, 78
 Thomas D., Maraston C., Bender R., Mendes de Oliveira C., 2005,
ApJ, 621, 673
 Tremonti C. A. et al. 2004, *ApJ*, 613, 898
 van der Wel A., 2008, *ApJ*, 675, L13
 van Dokkum P. G., 2005, *AJ*, 130, 2647
 Veilleux S., Osterbrock D. E., 1987, *ApJS*, 63, 295
 Yi S. K. et al. 2005, *ApJL*, 619, L111
 Yoon J. H., Schawinski K., Sheen Y.-K., Ree C. H., Yi S. K., 2008,
ApJS, 176, 414
 York D. G. et al. 2000, *AJ*, 120, 1579

This paper has been typeset from a $\text{\TeX}/\text{\LaTeX}$ file prepared by the author.

Table 2. A catalogue of blue early-type galaxies

SDSS Object ID	RA	DEC	Redshift	M_r	$u - r$	Star Formation Rate ¹ ($M_\odot yr^{-1}$)	Emission Line Class ²
587722981736906813	11:30:57.9	-01:08:51.1	0.04802	-21.43	2.365	-	Seyfert
587722982272925748	11:23:27.0	-00:42:48.8	0.04084	-20.81	1.606	4.5	SF
587722982276923512	12:00:04.3	-00:45:34.5	0.04711	-21.08	2.088	-	AGN+SF
587722982299271230	15:23:47.1	-00:38:23.0	0.03747	-21.00	1.998	2.5	SF
587722983351582785	12:08:23.5	+00:06:37.0	0.04081	-21.50	2.038	3.5	SF
587722984440463382	14:26:13.0	+00:51:38.1	0.03193	-20.87	2.035	-	LINER
587724198282133547	01:41:43.2	+13:40:32.8	0.04539	-21.81	1.432	12.	SF
587724199351812182	01:03:58.7	+15:14:50.1	0.04176	-21.40	2.261	7.0	SF
587724199355285539	01:36:19.4	+14:39:24.6	0.03369	-20.80	2.310	-	AGN+SF
587724231570817120	01:44:26.2	+13:09:35.5	0.04502	-20.93	2.152	-	AGN+SF
587724242298077193	02:25:22.1	-07:51:06.1	0.03919	-20.79	2.243	-	AGN+SF
587724650327113796	11:26:40.7	-01:41:37.6	0.04671	-21.95	1.857	-	LINER
587725491599835179	17:18:56.0	+57:22:18.8	0.03160	-20.98	1.993	-	AGN+SF
587725550139408424	12:35:02.6	+66:22:33.4	0.04684	-21.67	1.959	6.1	SF
587725550675755071	12:22:49.1	+66:51:45.3	0.03222	-21.66	2.270	-	-
587725551199322281	08:35:04.2	+52:49:53.5	0.04454	-21.94	2.402	-	-
587725773459554601	08:07:01.7	+45:42:29.3	0.04939	-21.56	2.361	-	-
587725773460733977	08:15:50.5	+47:48:39.6	0.04029	-21.31	2.185	-	AGN+SF
587725979615559791	08:36:14.9	+52:12:09.1	0.04809	-20.77	1.906	-	Seyfert
587725981226107027	08:29:09.1	+52:49:06.9	0.04842	-21.00	1.835	2.1	SF
587726014009573396	14:11:17.7	+01:16:31.0	0.02499	-20.71	2.299	-	AGN+SF
587726016149454996	13:02:10.8	+03:06:23.8	0.04724	-22.37	2.065	-	AGN+SF
587726031175548968	12:06:47.2	+01:17:09.8	0.04124	-21.18	2.207	1.2	SF
587726031691514020	08:55:50.3	+00:49:52.1	0.04171	-20.90	2.031	-	AGN+SF
587726032249749558	12:11:10.8	+02:15:19.9	0.01981	-20.71	2.266	-	-
587726032780066885	11:11:06.9	+02:28:48.0	0.03514	-20.87	2.259	-	Seyfert
587726033307238543	09:42:07.7	+02:28:05.1	0.04825	-21.40	2.361	-	Seyfert
587726033873862745	14:14:32.1	+03:11:24.9	0.02691	-21.82	2.334	-	-
587726033878122590	14:53:40.0	+02:55:14.4	0.04447	-20.84	1.876	-	AGN+SF
587726100953432183	15:17:19.7	+03:19:18.9	0.03749	-20.74	2.131	0.73	SF
587727178995204109	01:22:09.2	-09:53:18.8	0.04273	-21.93	2.394	-	-
587727180061999117	00:17:34.9	-09:32:36.1	0.02237	-21.58	2.388	-	-
587727180070715469	01:38:22.3	-08:58:31.4	0.04240	-20.80	2.054	-	-
587727221414494275	00:09:07.9	+14:27:55.8	0.04141	-21.42	2.219	-	Seyfert
587727221944746290	23:06:54.9	+14:11:30.3	0.03992	-21.11	2.298	-	AGN+SF
587727221949005979	23:47:03.8	+14:50:30.4	0.02217	-20.82	2.157	-	Seyfert
587727225693667361	00:32:45.2	-10:27:03.6	0.03833	-21.51	2.353	-	-
587727227846983785	01:26:49.9	-08:29:27.2	0.04968	-21.92	2.355	-	-
587727943497613319	10:04:38.7	+01:53:22.5	0.03034	-21.02	2.324	-	-
587728664506794118	08:29:57.5	+44:56:24.6	0.04271	-21.95	2.389	-	-
587728879266562060	10:16:28.4	+03:35:02.7	0.04848	-21.72	2.380	6.1	SF
587728905563603159	07:56:49.9	+34:49:52.6	0.04096	-21.06	2.039	-	AGN+SF
587728920059183194	14:43:05.3	+61:18:38.6	0.04796	-21.60	1.344	-	AGN+SF
587728947978436717	10:42:32.3	-00:41:58.3	0.04981	-20.82	2.048	-	-
587728948511637597	10:08:47.8	-00:16:11.3	0.04536	-22.07	2.239	-	AGN+SF
587728949049557028	10:18:06.7	+00:05:59.7	0.04840	-21.65	2.307	-	Seyfert
587728949584658573	10:02:22.5	+00:33:31.0	0.04424	-20.89	2.221	-	AGN+SF
587729157894832296	13:18:37.5	+03:59:42.4	0.04574	-20.79	2.312	-	AGN+SF
587729159518945292	15:22:01.9	+03:45:06.3	0.03714	-22.20	2.424	-	AGN+SF
587729160046510114	13:57:07.5	+05:15:06.8	0.03967	-21.86	2.158	6.6	SF
587729227152752660	16:03:44.5	+52:24:12.5	0.04322	-20.74	2.216	-	-

Table 2 (cont'd)

SDSS Object ID	RA	DEC	Redshift	M_r	$u - r$	Star Formation Rate ¹ ($M_\odot yr^{-1}$)	Emission Line Class ²
587729227683659793	14:51:15.7	+62:00:14.6	0.04306	-21.45	2.173	3.9	SF
587729387675844667	08:51:35.6	+47:33:27.6	0.02910	-22.25	2.415	-	AGN+SF
587729407542624367	16:43:23.1	+39:48:23.2	0.03024	-21.75	2.350	-	Seyfert
587729408611647550	16:10:51.8	+48:54:39.2	0.04504	-20.94	1.995	-	Seyfert
587729408622723373	17:23:24.9	+27:48:46.3	0.04845	-21.46	2.017	3.2	SF
587729751674323201	17:04:08.7	+31:29:02.4	0.03304	-21.27	2.318	-	AGN+SF
587729778516820024	14:06:56.4	-01:35:41.0	0.02916	-21.37	2.127	5.7	SF
587729778520817884	14:43:18.6	-01:15:12.5	0.04982	-21.63	2.364	-	-
587730773351006383	23:51:29.1	+14:04:06.2	0.03938	-21.25	2.029	-	Seyfert
587730816286785593	22:15:16.2	-09:15:47.6	0.03843	-21.61	1.707	21.0	SF
587731172234428781	21:14:52.4	-00:58:39.9	0.04402	-21.95	2.415	-	-
587731185117954089	22:08:06.1	-00:54:25.0	0.03797	-20.77	2.167	-	-
587731186744950905	00:38:14.7	+00:12:37.5	0.04440	-20.84	2.311	-	AGN+SF
587731187267403859	22:26:14.6	+00:40:04.1	0.03642	-22.04	2.340	-	-
587731500261834946	10:54:37.9	+55:39:46.0	0.04787	-20.89	1.976	6.5	SF
587731501332430930	10:06:04.3	+53:42:53.5	0.04427	-21.01	1.613	-	AGN+SF
587731512617402577	03:01:26.2	-00:04:25.5	0.04285	-21.10	2.156	3.2	SF
587731513696845940	03:53:34.8	+00:48:50.5	0.03785	-20.79	1.753	-	AGN+SF
587731514229784683	03:17:49.3	+01:13:37.2	0.03685	-21.26	2.200	-	Seyfert
587731514501365802	03:46:12.1	+01:07:15.9	0.03805	-21.09	2.318	-	-
587731521207730241	09:13:23.7	+43:58:34.2	0.04292	-21.45	2.176	14.0	SF
587731680111099933	07:54:01.2	+29:25:14.5	0.03608	-20.71	2.296	-	LINER
587731874461974650	08:12:25.5	+37:43:48.8	0.03852	-21.07	1.448	-	AGN+SF
587731887347662946	08:21:49.6	+39:14:49.6	0.02821	-20.74	2.022	-	AGN+SF
587731887888990283	09:00:36.1	+46:41:11.4	0.02748	-21.30	2.200	-	-
587731889505632389	12:20:37.4	+56:28:46.2	0.04381	-20.84	2.238	0.53	SF
587732053246017714	09:18:55.2	+42:00:13.0	0.04113	-21.74	2.425	-	-
587732054318645354	09:05:37.2	+41:05:32.2	0.04137	-21.70	2.342	-	LINER
587732134844366940	11:06:21.4	+50:23:16.8	0.03988	-20.91	2.011	-	Seyfert
587732135382089788	11:17:33.3	+51:16:17.7	0.02767	-21.40	2.332	-	-
587732135921057870	11:47:41.7	+52:26:55.8	0.04816	-21.92	2.226	-	AGN+SF
587732136457011245	11:33:39.1	+52:40:28.6	0.04913	-20.80	2.163	-	-
587732157389013064	07:54:20.6	+25:51:33.2	0.04167	-21.06	2.011	1.7	SF
587732469849653424	08:29:30.0	+31:40:31.7	0.01828	-20.73	2.090	-	AGN+SF
587732471463411876	08:53:11.4	+37:08:06.5	0.04980	-21.59	2.063	10.0	SF
587732484375838770	15:33:44.5	+39:13:42.0	0.04034	-21.26	2.283	-	-
587732577238974514	11:07:16.6	+06:18:08.9	0.02915	-22.24	2.502	-	-
587732580982521898	11:19:07.6	+58:03:14.4	0.03250	-21.40	2.171	-	-
587732582592479319	11:05:59.0	+58:56:45.8	0.04765	-22.02	2.435	-	Seyfert
587732701792895177	10:48:07.9	+06:18:19.4	0.04196	-21.13	2.278	-	AGN+SF
587732769982906490	12:20:23.1	+08:51:37.1	0.04894	-20.88	2.086	3.6	SF
587732771580149928	10:16:58.0	+08:39:16.1	0.02775	-20.92	2.334	-	-
587732772653957258	10:17:06.8	+09:36:22.6	0.04393	-21.09	1.588	-	AGN+SF
587733081351258168	12:40:55.5	+55:27:15.2	0.03175	-21.29	2.357	-	-
587733195160485975	13:05:25.8	+53:35:30.3	0.03812	-21.68	2.212	-	-
587733197845561478	13:19:31.5	+55:17:50.5	0.03813	-21.48	2.325	-	AGN+SF
587733397559902223	14:01:55.2	+51:31:10.3	0.04122	-20.91	2.291	-	Seyfert
587733398642688031	15:47:44.1	+41:24:08.3	0.03260	-21.04	2.156	-	Seyfert
587733410445131853	14:02:24.5	+51:41:13.1	0.04120	-21.75	2.388	-	-
587733411518808182	14:02:48.8	+52:30:00.8	0.04361	-20.77	1.893	1.4	SF
587733412055941186	14:07:47.2	+52:38:09.7	0.04381	-20.78	1.812	4.2	SF

Table 2 (cont'd)

SDSS Object ID	RA	DEC	Redshift	M_r	$u - r$	Star Formation Rate ¹ ($M_\odot yr^{-1}$)	Emission Line Class ²
587733412064788620	15:50:00.5	+41:58:11.2	0.03391	-20.80	1.879	3.6	SF
587733412068261940	16:19:32.4	+36:31:16.3	0.03636	-21.16	2.225	-	AGN+SF
587733432459788474	16:51:16.7	+28:06:52.5	0.04724	-21.59	1.921	4.0	SF
587733604808524062	16:56:20.3	+32:10:27.4	0.03671	-21.32	2.340	-	AGN+SF
587734303266308145	22:05:15.4	-01:07:33.4	0.03172	-21.38	2.011	-	LINER
587734622698602943	07:47:23.1	+22:20:41.3	0.04549	-20.90	2.256	0.45	SF
587734622700831054	08:03:29.3	+25:44:18.6	0.04679	-21.07	2.295	-	-
587734622705811566	08:44:37.8	+32:54:23.2	0.03154	-20.91	2.086	-	LINER
587734891674796073	11:17:59.8	+08:44:35.0	0.04541	-20.74	2.255	-	-
587734892755419193	12:21:23.3	+09:50:53.0	0.04667	-21.45	2.354	-	-
587734893287374941	11:35:39.9	+10:10:02.8	0.04199	-21.39	2.349	-	-
587734949655740512	08:38:43.5	+07:48:23.8	0.02955	-21.67	2.356	-	-
587735044152623112	09:04:55.3	+33:57:22.1	0.04354	-21.57	2.376	-	-
587735044686348347	08:36:01.5	+30:15:59.1	0.02561	-21.10	2.268	-	-
587735348575535135	12:23:23.8	+15:10:18.8	0.04238	-22.04	2.252	-	AGN+SF
587735697525637156	14:30:51.1	+53:54:28.0	0.04336	-21.74	2.348	-	AGN+SF
587735742615388296	15:53:35.6	+32:18:20.6	0.04985	-21.07	1.789	3.2	SF
587736477058138251	15:05:43.8	+08:47:18.9	0.04632	-21.07	2.282	-	-
587736477586554950	13:47:47.7	+11:16:27.0	0.03942	-21.20	1.911	5.5	SF
587736478661279818	13:57:13.2	+12:01:16.8	0.02077	-21.69	2.142	-	-
587736542015127621	13:52:00.4	+08:52:55.3	0.03766	-21.48	1.909	-	AGN+SF
587736584980463705	16:44:30.8	+19:56:26.7	0.02300	-20.71	1.873	5.2	SF
587736619863965778	16:21:19.5	+24:39:59.9	0.03786	-21.03	2.170	-	-
587736783604482120	15:47:44.4	+37:12:18.1	0.03967	-22.24	2.447	-	-
587736941986250794	15:06:24.2	+32:25:51.0	0.04339	-21.20	2.236	-	LINER
587737808499245260	08:37:15.4	+55:54:29.5	0.03790	-20.80	2.291	-	-
587738067267878973	07:59:12.4	+53:33:26.0	0.03479	-20.92	1.657	13.0	SF
587738067269255432	08:10:20.1	+56:12:26.3	0.04623	-20.78	2.130	1.0	SF
587738195577929986	07:58:53.7	+52:19:30.8	0.04070	-21.05	2.161	-	-
587738568174534706	13:34:09.4	+13:16:51.0	0.04409	-22.03	2.246	-	AGN+SF
587738570849845253	12:08:37.4	+16:08:34.0	0.02265	-21.65	2.401	-	-
587738574070939706	13:24:58.2	+39:07:06.4	0.03726	-20.78	2.284	-	AGN+SF
587738618094026755	10:19:08.7	+34:34:09.3	0.03525	-21.41	2.350	-	-
587738946685304841	12:37:15.7	+39:28:59.3	0.02035	-20.92	2.156	-	LINER
587738947194519672	07:56:36.3	+18:44:17.7	0.03988	-21.53	2.088	3.9	SF
587739096454332452	12:38:52.8	+36:32:05.7	0.04976	-20.91	2.173	-	-
587739115234394179	07:56:08.7	+17:22:50.5	0.02899	-20.73	2.211	1.6	SF
587739132429205602	15:57:21.4	+24:24:28.0	0.04341	-21.60	2.221	-	AGN+SF
587739156580597805	10:01:01.9	+31:12:17.1	0.04379	-21.17	2.091	-	Seyfert
587739165700653215	16:09:07.3	+21:52:03.8	0.03127	-20.99	2.190	-	AGN+SF
587739166237851766	16:13:25.6	+21:54:33.9	0.03193	-21.75	2.423	-	-
587739303685193778	13:15:37.6	+34:02:31.5	0.03408	-20.89	2.218	-	-
587739406262468657	15:18:09.6	+25:42:11.5	0.03260	-20.85	1.960	6.6	SF
587739406268039264	16:07:54.0	+20:03:03.8	0.03165	-20.73	1.487	4.8	SF
587739506086707246	13:26:20.8	+31:41:59.9	0.04999	-21.89	1.930	6.7	SF
587739647814139970	10:20:34.9	+29:14:10.8	0.04846	-20.96	1.998	1.0	SF
587739648357826596	11:31:22.0	+32:42:22.9	0.03368	-21.61	2.015	6.3	SF
587739809414905903	14:30:58.8	+22:39:45.5	0.04456	-20.79	2.235	-	-
587739810496512078	15:44:51.5	+17:51:22.5	0.04521	-21.32	1.994	3.7	SF
587739811571957865	16:01:28.1	+17:14:25.9	0.03602	-21.65	2.427	-	-
587739814246023211	16:25:38.1	+16:27:18.1	0.03432	-22.28	2.430	-	LINER

Table 2 (cont'd)

SDSS Object ID	RA	DEC	Redshift	M_r	$u - r$	Star Formation Rate ¹ ($M_\odot yr^{-1}$)	Emission Line Class ²
587739814778634376	15:49:59.8	+21:11:22.7	0.03493	-20.74	2.184	-	AGN+SF
587739815852965987	15:56:33.7	+21:17:20.7	0.01470	-20.95	2.310	-	-
587739828213055504	16:05:22.7	+16:11:53.6	0.03374	-21.74	2.370	-	-
587739828749730189	16:04:39.4	+16:44:43.6	0.04599	-20.74	2.308	0.54	SF
587741420558221629	07:52:57.1	+13:30:02.9	0.04926	-20.74	2.310	-	AGN+SF
587741490887852274	07:56:49.3	+13:53:49.8	0.04501	-21.49	2.258	-	AGN+SF
587741490904105107	10:25:24.7	+27:25:06.3	0.04973	-20.98	2.256	3.1	SF
587741532763324554	07:55:23.3	+12:57:11.6	0.04413	-21.29	2.331	-	AGN+SF
587741600427147349	13:17:39.6	+25:32:46.3	0.04563	-21.12	2.118	-	AGN+SF
587741601491845160	11:45:03.7	+26:49:39.8	0.03011	-21.24	2.293	-	Seyfert
587741602572730395	12:58:35.2	+27:35:47.0	0.02572	-21.79	1.977	-	AGN+SF
587741708333940769	09:40:44.5	+21:14:03.4	0.02442	-20.72	2.156	-	Seyfert
587741709410369692	10:05:19.9	+23:49:01.2	0.04559	-20.74	2.316	-	AGN+SF
587741709955563564	11:28:19.9	+27:37:19.6	0.03215	-20.71	2.320	-	Seyfert
587741723360165908	12:54:53.7	+28:25:01.1	0.02465	-20.80	2.280	-	AGN+SF
587741816781209661	09:48:09.2	+20:18:32.8	0.03964	-21.34	2.084	-	Seyfert
587741828579983420	10:26:39.5	+21:48:11.6	0.04238	-21.68	2.387	-	-
587742191508586532	11:06:47.9	+24:55:47.1	0.04851	-21.64	2.132	-	AGN+SF
588007005234856197	08:17:56.3	+47:07:19.5	0.03901	-21.06	2.309	8.1	SF
588007005259038814	14:57:46.5	+59:20:32.7	0.03922	-21.91	2.335	-	-
588009371761573965	11:13:06.6	+61:38:18.0	0.04543	-21.42	2.330	-	LINER
588010135730782222	09:24:29.6	+53:41:37.8	0.04590	-20.80	1.997	0.63	SF
588010360691490829	11:10:38.2	+05:56:03.8	0.04147	-21.16	2.260	-	-
588010878765826140	13:01:41.4	+04:40:49.9	0.03836	-21.40	2.101	1.5	SF
588010879306432606	13:36:12.2	+04:44:24.3	0.03434	-21.57	2.380	-	LINER
588011102644207665	16:02:00.2	+47:52:54.8	0.04309	-21.27	2.304	-	AGN+SF
588011125186691149	12:06:17.0	+63:38:19.0	0.03974	-21.26	1.686	18.0	SF
588011216986505290	13:13:49.1	+60:41:04.8	0.03809	-20.75	2.169	-	-
588011216991289349	14:32:22.7	+56:51:08.4	0.04302	-21.74	1.864	6.1	SF
588011218063392805	14:10:13.0	+59:15:23.6	0.04285	-21.65	2.323	-	-
588013383806091298	09:39:14.8	+45:21:57.3	0.04264	-20.86	2.310	-	-
588015508201472181	00:53:29.4	-00:40:38.4	0.04377	-20.86	2.317	-	-
588015509815558168	01:25:02.9	+00:26:39.7	0.02875	-21.59	2.034	-	AGN+SF
588016840704131407	07:46:02.4	+18:43:01.7	0.04625	-21.86	2.420	-	AGN+SF
588017110752165893	10:46:07.3	+44:43:28.9	0.04718	-21.95	2.327	-	AGN+SF
588017567636652100	12:14:15.4	+13:30:55.8	0.04295	-20.77	2.311	-	-
588017604156784724	14:14:33.2	+40:45:22.9	0.04185	-20.86	1.614	5.2	SF
588017604680417320	11:29:48.7	+44:13:49.9	0.04539	-22.13	2.429	-	LINER
588017606292865048	11:52:05.0	+45:57:06.6	0.04316	-20.72	1.842	1.7	SF
588017626159906869	13:17:38.0	+43:48:38.3	0.02798	-21.07	1.933	-	AGN+SF
588017627759444009	10:55:46.8	+44:02:58.8	0.03715	-21.43	2.270	-	LINER
588017627778580560	14:53:23.4	+39:04:13.6	0.03153	-20.88	2.134	1.2	SF
588017702392430629	11:48:57.8	+11:27:18.4	0.04321	-20.71	2.053	-	AGN+SF
588017703476658186	13:26:37.5	+11:52:10.2	0.04624	-22.49	2.527	-	-
588017704030961755	16:07:18.7	+07:10:51.3	0.04669	-21.13	2.227	-	AGN+SF
588017728158695498	13:26:00.9	+06:13:23.3	0.03961	-21.35	2.347	-	-
588017947211006028	13:37:09.3	+39:52:24.5	0.04894	-21.51	2.293	-	-
588017978342375556	09:46:08.4	+32:53:50.2	0.03680	-20.78	2.231	-	AGN+SF
588017978903232631	14:17:32.6	+36:20:19.1	0.04712	-20.93	1.916	1.6	SF
588017979974418577	13:50:34.6	+38:45:06.1	0.04918	-20.74	2.170	-	-
588017979975008316	13:56:49.2	+38:18:50.8	0.03431	-20.77	2.036	-	AGN+SF

Table 2 (cont'd)

SDSS Object ID	RA	DEC	Redshift	M_r	$u - r$	Star Formation Rate ¹ ($M_{\odot} yr^{-1}$)	Emission Line Class ²
588017990148816933	12:59:48.6	+08:55:57.9	0.04620	-21.28	2.177	-	LINER
588017991233110227	14:37:33.0	+08:04:43.0	0.04987	-21.62	2.353	3.6	SF
588017991773978739	15:14:29.9	+07:35:46.8	0.04484	-20.79	2.042	-	-
588018091080351786	15:58:25.4	+32:58:07.7	0.04798	-21.87	2.295	-	-
588018254297038899	16:18:18.7	+34:06:40.1	0.04733	-21.58	2.307	2.9	SF
588023239671087134	09:13:20.7	+17:38:27.7	0.02554	-21.33	2.238	-	-
588295840177061984	12:19:05.9	+48:49:27.7	0.04468	-20.85	2.151	-	AGN+SF
588295842320744617	11:25:07.3	+49:42:02.6	0.04997	-21.42	2.382	-	-
588297863102988421	08:43:46.7	+31:34:52.6	0.04756	-20.70	2.110	7.3	SF
588297864718909472	09:30:31.3	+39:17:50.0	0.04605	-21.87	2.143	-	-
588848899365601360	10:26:54.6	-00:32:29.4	0.03463	-21.38	2.137	7.6	SF

¹The aperture-corrected H α SFR. This is given only for the objects classified as starforming by the emission line diagrams.

² Emission line classification, objects that do not have S/N > 3 in the four main lines are given as '-'.²